

Formation of TiO₂ Nanotubular Layers on Ti-6Al-4V Based Dental Implants for Inhibiting Biofilm Growth

SLAMET^{1,*}, BOY M. BACHTIAR², PRASWASTI P.D.K. WULAN¹, BILLY APRIANTO¹ and MUHAMMAD IBADURROHMAN¹

¹Department of Chemical Engineering, Faculty of Engineering, Universitas Indonesia, Depok 16424, Indonesia

²Department of Oral Biology Department, Faculty of Dentistry, Universitas Indonesia, Jakarta 10430, Indonesia

*Corresponding author: E-mail: slamet@che.ui.ac.id

Received: 19 September 2019;

Accepted: 7 March 2020;

Published online: 27 June 2020;

AJC-19910

Modification of Ti-6Al-4V through electrochemical anodization method has been investigated on the purpose of generating TiO₂ nanotube arrays (TiNTAs) on the surface of Ti-6Al-4V films. The as-anodized samples were calcined in an atmospheric furnace at various temperatures, in the range of 500-800 °C. The evaluation of biofilm inhibition was performed by an *in vitro* method with *Streptococcus mutans* as a bacterium model. FE-SEM imaging confirmed the successful formation of TiO₂ nanotube arrays while XRD results implied a phase transformation from anatase to rutile when the calcination temperature was around 600-650 °C with average crystallite size of 18 nm. Calcination temperature is one of determining factors in the adjustment of crystallinity and morphology of TiO₂, which in turn affects its capability to suppress biofilm formation. This study revealed that the best sample for biofilm inhibition was calcined at 600 °C with a crystallite phase of mostly anatase. This sample managed to improve antibacterial activity of up to five times as compared to the unmodified Ti-6Al-4V. The output of this study is expected to give some insight on a promising alternative for preventing the formation of harmful biofilm on dental implants.

Keywords: Biofilms, Dental implant, Surface modification, TiO₂ nanotubes.

INTRODUCTION

The use of dental implants has been widely recognized in the global community in line with the increasing of common dental problems, especially for restoring dentition defects and anodontia [1]. Although the rate of success of dental implants for their purpose were duly acknowledged, some limitations in the long term prognosis of dental implants, such as peri-implant infection (peri-implantitis), still need to be addressed. Peri-implantitis, which is caused by colonization of bacteria infecting the gums and alveolar around the dental implants, may lead to eventual implant failure and short term longevity which requires revision surgery [2-5].

Dental implants are typically made from commercially pure titanium (cpTi) or titanium alloys [6], especially Ti-6Al-4V [7-9], which are deemed suitable and compatible for biomedical applications [10]. The alloy of Ti-6Al-4V (90% Ti, 6% Al, 4% V) offers excellent corrosion resistance and the ability to deform super plastically due to its low density and good biocom-

patibility that make it preferable to substitute a complex shape hard tissue [11]. The spontaneous passivation of this alloy forms a thin outer layer, predominantly consists of amorphous or poorly recrystallized TiO₂ with thickness of 2-5 nm that protects the bulk material from corrosion and makes it bioinert [12].

TiO₂ is found in three main crystallographic forms in the environment, namely anatase, rutile and brookite. However, among these three, anatase is arguably the most photocatalytically active as compared to the amorphous or unstable phases of TiO₂ [13,14]. Due to the non-selective nature of excitons generated from photoexcitation of anatase, it covers a wide scope of applications, including bacteria disinfection which has been an important topic for discussions for the past decade, particularly that which involves *Escherichia coli* [15]. The photocatalytic process would generate hydroxyl radicals that attack the cell walls of bacteria, leading to massive fluid extraction and eventual death. The presence of hydroxyl radicals in the body is deemed harmless because it would directly attack the

bacterial cells and typically has fast life-cycle in human body [16].

From a microbial physiology aspect, oral microbial communities are classical examples of biofilms [17]. *Streptococcus mutans* are the most prevalent species in humans that are commonly found in healthy periodontal individuals and are related to mucosal surfaces; besides it can contribute to the coaggregation of pathogenic bacteria such as *Porphyromonas gingivalis* [18]. Oral streptococci, especially *Streptococcus mutans*, are thus considered as the pioneer colonizers and might participate in the process, which can lead to implant failure in the long run [18].

Some surface modifications of titanium have been studied including titanium plasma spraying (TPS), plasma sprayed hydroxyapatite coating, alumina coatings and biomimetic calcium phosphate coating [19]. Recently, the anodization technique of titanium leading to the formation of titanium dioxide nanotube arrays (TiNTAs) on the surface has attracted much attention [12]. The anodized TiNTAs surface possesses promising potentials for biomedical application, since they are able to increase the growth of hydroxyapatite, increasing osteoblast cell adhesion and desirable functions, and influence cellular behavior to enhance tissue integration [12]. Antibacterial properties are also crucial for dental implant materials in order to minimize the possibility of infection caused by bacteria colonization. Several studies have been done to optimize the anti-bacterial properties of Ti-6Al-4V. The anodized Ti-6Al-4V exhibit antibacterial properties with a thin film of anatase under UV treatment [15]. However, the antibacterial properties of thin films are still being discussed, because the thin film of anatase has the possibility to exfoliate. Hence, to obtain a stable antibacterial film, optimization of TiNTAs' morphology and its crystallite structure is required.

Optimization of TiNTAs' crystallite structure and morphology on the surface of Ti-6Al-4V in terms of thermal treatment has not been extensively investigated. Therefore, this present study is intended to investigate the effect of calcination temperature on the morphology and crystallite structure of TiNTAs as well as their resultant antibacterial properties. *Streptococcus mutans* were used as a model of biofilm generated on the surface of implants in order to evaluate the effectiveness of modified Ti-6Al-4V in inhibiting biofilm formation.

EXPERIMENTAL

Preparation of specimen: Prior to anodization, titanium alloy grade 5 (specially made for dental implants with 6% Al and 4% V) were cut into 40 × 8 × 7 mm. The samples were ground through successive grades of silicon carbide paper (CC 1500 CW). Upon grinding, the samples were degreased with detergent in TELSONIC ultrasonic bed and chemically polished by a mixture of HF, HNO₃ and water with volume ratio of 1:3:6. The substrate was then rinsed by deionized water.

Electrolyte solution used in the anodization method was a mixture of glycerol, water and NH₄F (0.5% wt) with 25% water content. Ti-6Al-4V was assigned as the working electrode with Pt (3 mm thickness) as the counter electrode. The distance between the two electrodes was maintained at 35 mm. Anodi-

zation process was evaluated in a beaker glass in 60 mL of electrolyte solution. A fixed potential of 30 V was applied for 2 h at room temperature with magnetic agitation. The material was then rinsed with deionized water and dried in the open air after the anodization process. The drying is followed by atmospheric calcination at various temperature (500-800 °C) for 3 h. The specimens were then cut into 15 × 8 × 7 mm based on the test template.

Surface characterization: The surface morphology and elemental composition of the modified Ti-6Al-4V were characterized by FE-SEM (Hitachi S-4700) at EHT of 20 kV, equipped with energy dispersive X-ray spectroscopy (EDS). In order to determine the crystallite structure of specimens, X-ray diffraction (XRD) characterization was performed. The XRD patterns were obtained using Shimadzu XRD-7000 with Cu anode tube ($\lambda = 0.154184$ nm), operated at 40 kV and current 20 mA, with the range of 2 θ angle values 20° to 70°. The crystallite size of the specimen was estimated from FWHM of XRD by Scherrer's equation.

Biofilm inhibition test: Biofilm inhibition tests were performed on non-anodized and anodized Ti-6Al-4V specimens. Prior to the inhibition test, *Streptococcus mutans* Xc (serotype C) was grown overnight in brain heart infusion (BHI) broth (Difco Laboratories) at 37 °C in air atmosphere supplemented with 5% CO₂ (v/v) for 18 h, until they reached the stationary phase of bacterial growth. For biofilm assay, the disks were subjected to ultrasonic cleaning and autoclaving. After immersed in 200 μ L of filter (pore size 0.22 μ m²), sterilized saliva (collected from a volunteer with proper documented consent as per medical guidelines) for 30 min at 37 °C, the disks were washed three times with phosphate buffer saline (PBS: Sigma-Aldrich; pH 7.0). Ti-6Al-4V and TiNTAs/Ti-6Al-4V were placed on the bottom of a 24-well plates (Iwaki, Japan) and exposed to bacterial suspension (2 × 10⁶ cfu/mL) in brain heart infusion (BHI) broth with 1% sucrose and the bacterium was grown under static conditions (5% CO₂ at 37 °C). Following each incubation time (6, 8 and 24 h), media containing dispersal cells were discarded. Then, the wells and the disks were washed three times with 150 μ L of sterile PBS to remove non-adherent cells. The biofilms were then stained with 100 μ L (1%) crystal violet for 15 min and washed three times with PBS to remove unbound crystal violet dye and dried at room temperature. The stains were released from the biofilms by adding 1 mL of absolute ethanol, and the wells were incubated on a rocking platform for 20 min at room temperature. Absorbance was recorded at 590 nm, using ELISA reader. Each biofilm assay was run in duplicate in two separate independent experiments. Data are expressed as means and standard deviations of triplicate experiments by using Student's *t*-test. A *p* < 0.05 was considered as a significant level of bacteria breeding models performed on BHI broth for the growth of *S. mutans* Xc (serotype C). As-anodized Ti-6Al-4V specimens were exposed to UV (ELITE electronic fluorescent lights, $\lambda = 365$ nm) for 10 h in order to activate antibacterial activity of TiNTAs. The UV illumination was done inside a box equipped with aluminum foil for light reflection. The irradiated specimens were then sterilized and coated with saliva proteins that have been previously screened. Similar to

the Ti-6Al-4V specimens, the 24-well plate was coated with 120 μ L saliva proteins on the bottom and then incubated at 37 °C. The Ti-6Al-4V specimens and the 24-well plate were washed with PBS (pH 7.2).

Ti-6Al-4V specimens that have been coated with saliva proteins inserted into the test template (well plate) that had also been coated with saliva proteins. A 500 μ L of BHI broth that has been overgrown with bacteria incorporated into the test template, sealed and then purged with 30% CO₂. Then, the test template was incubated at 37 °C. Data were collected after 6, 8 and 24 h after incubation. The supernatant fluid was removed and the template was separated. Then, Ti-6Al-4V specimens were then inserted into 1 mL PBS solution in Eppendorf tubes. The biofilms formed were separated from the materials using vortex Bio-Rad BR-2000 for 30 s and centrifuged using Thermo-centrifuge with Legend Micro 17 with 10.000/min speed for 2 min. The supernatant solution caused by centrifugation was then eliminated. A pellets solution at the bottom of tube was collected and dried, then dripped with 500 μ L crystal violet for 10 min. Afterwards, excess crystal violet solution which is not attached to Ti-6Al-4V specimens was eliminated. On the other hand, attached crystal violet solution was cleaned and mixed with 400 μ L 96% alcohol. The previous 200 μ L mixed solution was poured into the 96-well plate to estimate the optical density values with ELISA microplate reader. Concentration of biofilm attached on the base plate can also be read at the same plate. Total plate count analysis was also performed by growing bacteria in 5 μ L of the solution of bacteria, which attached on the material.

RESULTS AND DISCUSSION

Surface characterization: The surface morphology of untreated (non-anodized) Ti-6Al-4V can be seen in Fig. 1a, showing a compact surface. After anodization and thermal treatment, the surface porosity is enhanced significantly, indicating that nanotubular structure has been formed successfully (Fig. 1b). Fig. 1b also shows some spots of rugged surface in the samples indicated by dark part (red circled). We conjectured that the dark parts were the structure of β -phase material. The various contours of surface were generated between the structure of α -phase and β -phase due to the growth of TiO₂ nanotube arrays (TiNTAs) and its wall thickening on the α -phase structure. It was reported that rugged surface is affected by α - β phase as a result of the presence of Al and V component in the material. The α -phase is the phase where the aluminium portion plays a

role as the dominant element in the balance of alloy, while β -phase is predominantly induced by vanadium [20].

Fig. 2a-f shows the surface morphology of anodized Ti-6Al-4V, calcined at various temperatures. The morphology evolution of the samples is apparent as the calcination temperature increases. For samples calcined at 500-625 °C, the nanotubular structure was intact after thermal treatment with similar morphology and dimension. Increasing the temperature up to 650 °C results in slight agglomeration on top of the nanotubes, leading to lower pore diameter. This is usually considered disadvantageous to photocatalytic process since the technical surface area becomes lower, interfering the accessibility of disinfection agents to the bacteria target. Further increase of calcination temperature destroys the nanotubular alignment in totality. The presence of TiO₂ nanotube layer is crucial for antibacterial activity because it ensures high surface area for the contact between hydroxyl radicals generated from photocatalytic process and the target bacteria.

Matytkina *et al.* [20] suggested that the growth of nanotubes film layer on the β phase of Ti-6Al-4V would lead to a heterogeneous growth and result in a larger diameter of the growing tubes. From the rightmost column of Table-1, it is apparent that the more β phase exists on Ti-6Al-4V alloy, the larger outer diameter of the growing tubes become, as visually confirmed by SEM imaging (Fig. 2a-d). Calcined at 500 °C, the outer diameter of the nanotubes was around 107.5 ± 41.2 while this value was found to be decreasing as the calcination temperature becomes higher.

TABLE-1
ELEMENTAL COMPOSITION OF
UNTREATED AND MODIFIED Ti-6Al-4V

Specimen ^a	Elements (wt%) ^b				Outer tube diameter size (nm) ^c
	Ti	Al	V	O	
Untreated Ti-6Al-4V ^d	89.49	6.10	4.30	0.11	–
Ti-6Al-4V.500	70.73	2.24	1.17	25.87	66-149
Ti-6Al-4V.600	67.08	2.41	0.84	29.69	54-115
Ti-6Al-4V.625	62.27	1.87	1.89	33.97	67-105
Ti-6Al-4V.650	60.21	2.78	0.92	36.09	69-99
Ti-6Al-4V.700	51.56	4.38	0.95	43.12	–
Ti-6Al-4V.800	61.81	2.10	0.75	35.36	–

^aThe right-most number denotes calcination temperature [°C];

^bPredicted by EDS; ^cPredicted by SEM; ^dObtained from reference method (ASTM E1477)

Table-1 provides the energy dispersive X-ray spectroscopy (EDS) characterization results, which show that Ti on untreated Ti-6Al-4V was oxidized as indicated by sharp increase of O element. Indeed, Al and V could have also been oxidized, generating a thin layer of stable oxides Al₂O₃ and V₂O₅. It is suggested that V₂O₅ thin layer could improve the stability of Ti-6Al-4V, while Al₂O₃ thin layer may decrease the photocatalytic properties of TiO₂ layer by interfering light absorption. However, Al₂O₃ layer might also play a role as a support for the photocatalytic process during operation. On the other hand, presence of Al₂O₃ and V₂O₅ thin layer might also be beneficial in affecting the band gap of TiO₂, leading to absorption of light of longer wavelength.

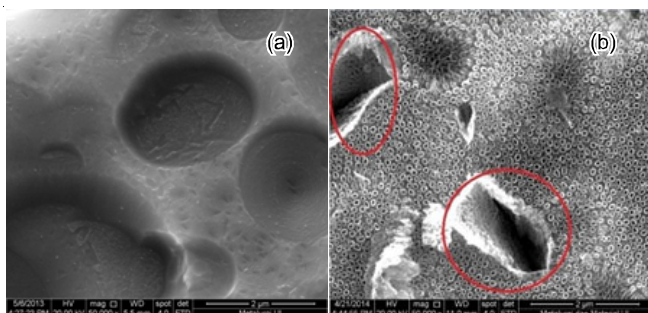


Fig. 1. FE-SEM image of (a) untreated Ti-6Al-4V, (b) TiNTAs β -phase (red circled) on modified Ti-6Al-4V

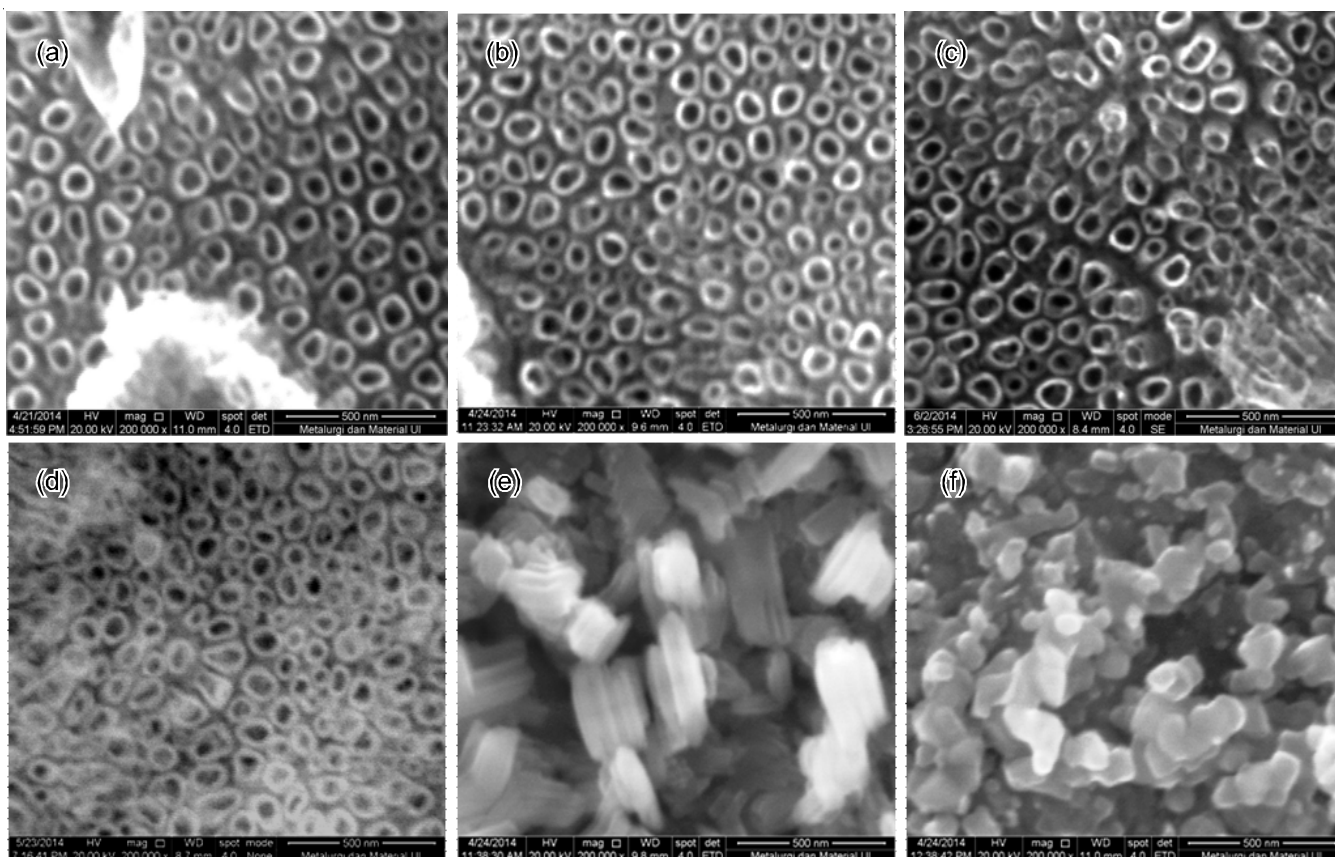


Fig. 2. FE-SEM image of anodized Ti-6Al-4V that calcined at (a) 500 °C, (b) 600 °C, (c) 625 °C, (d) 650 °C, (e) 700 °C, (f) 800 °C

Fig. 3 depicts the X-ray diffraction patterns of the modified Ti-6Al-4V samples calcined at various temperatures. In the cases of samples calcined at 500 and 600 °C, purely anatase nanotube layer is to be perceived on the plate surface, confirmed by the characteristic peaks at 2θ of around 25.3°, 38.0° and 48°. Increasing calcination temperature up to 625 °C and higher led to a phase transformation of titania from anatase to rutile, indicated by the presence of major peaks at 27°, 36° and 55°, which confirmed the diffraction characteristic of rutile crystallite phase. It is also observed that the diffraction peak for elemental Ti decreases with calcination temperature, which imply the growth of TiO₂ layer, regardless of whether or not nanotubes are present.

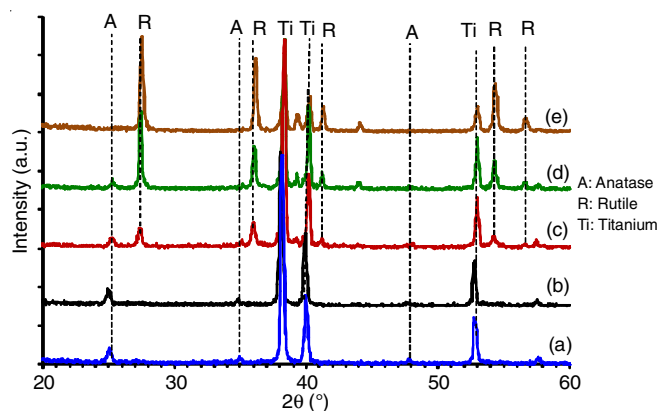


Fig. 3. XRD pattern of samples, calcined at (a) 500 °C, (b) 600 °C, (c) 625 °C, (d) 650 °C and (e) 700 °C

The anatase-rutile composition as well as the corresponding crystallite size can be estimated using Scherrer's equation, (eqn. 1). The anatase-rutile composition is calculated as follows:

$$x = \left(1 + 0.8 \frac{I_A}{I_R} \right)^{-1} \quad (1)$$

where x is the fraction of rutile phase, I_A and I_R are the X-ray spectrum intensity of anatase and rutile (a.u.). Furthermore, the crystallite size is calculated as follows:

$$t = \frac{0.9\lambda}{B \cos \theta} \quad (2)$$

where t is the average crystal size (nm), λ is the X-ray wavelength, B is the width of half-maximum peak (FWHM in radian unit) [21] and θ is diffraction angle in degree (°). The results of the calculation are presented in Table-2.

TABLE-2
CRYSTALLITE SIZES AND CRYSTALLITE
FRACTION OF MODIFIED Ti-6Al-4V

Specimen	Crystallite size (nm)*		Crystallite fraction* (%)	
	Anatase	Rutile	Anatase	Rutile
Ti-6Al-4V.500	18.08	–	100	–
Ti-6Al-4V.600	17.73	–	100	–
Ti-6Al-4V.625	18.27	18.04	59	41
Ti-6Al-4V.650	18.13	17.86	11	89
Ti-6Al-4V.700	–	17.59	–	100

*Calculated using Scherrer equation.

The results in Table-2 show that the crystallite size did not exhibit strong dependence on the calcination temperature. However, significant effects of calcination temperature can be seen in terms of the anatase-rutile composition. At 625 °C, the rutile structure began to rise, contributing 41% of the crystallite structure of the material. Increasing calcination further led to significant increase of the fraction of rutile. In fact, at 700 °C, the transformation has completed with no remaining anatase crystallite phase. This observation suggests that the phase transformation could be associated with the destruction of nanotubular structures when the calcination temperature is too high. Based on the assessments of morphology and crystallinity, samples calcined at 500, 600 and 625 °C are deemed suitable for bacterial disinfection process.

Biofilm inhibition test: Biofilm inhibition test was evaluated using modified Ti-6Al-4V calcined at 500, 600 and 625 °C *via in vitro* method with *Streptococcus mutans* as a model of implant's bacteria. Biofilm formation ratio is the ratio between the concentration of bacteria attached to the modified Ti-6Al-4V (calcined at 500, 600 and 625 °C) and the bottom well plate which is used as a test plate. This type of analysis is done to study the tendency of bacteria in attaching on the Ti-6Al-4V sample as compared to the control that is modelled on well plate as a container control. This comparison was performed in order to show the inhibition ability of biofilm formation by the implant material.

Fig. 4 shows that all modified samples exhibit bactericidal activities as compared to the unmodified Ti-6Al-4V specimen. The presence of TiO₂ nanotube arrays on the surface may facilitate effective inhibition of biofilm formation of *Streptococcus mutans*. In particular, modified sample calcined at 600 °C managed to inhibit film down to around 20% after 24 h. Biofilm inhibition performance was also evaluated by total plate count (TPC) analysis (Fig. 5). The results corroborate the previously mentioned data. It can be concluded from these tests that modified Ti-6Al-4V calcined at 600 °C is the best sample to inhibit the biofilm formation. This study confirms the importance of surface morphology and crystallinity of dental implant materials

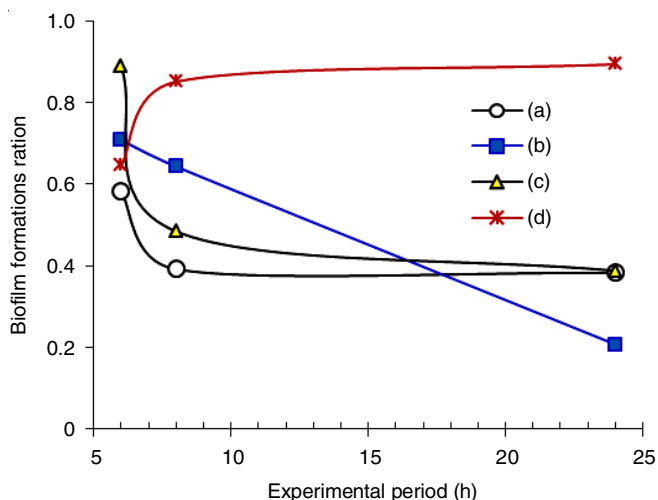


Fig. 4. Ratio of biofilm attached to the modified Ti-6Al-4V (compared to the bottom of well plate control bacteria) calcined at (a) 500 °C, (b) 600 °C, (c) 625 °C and (d) unmodified Ti-6Al-4V

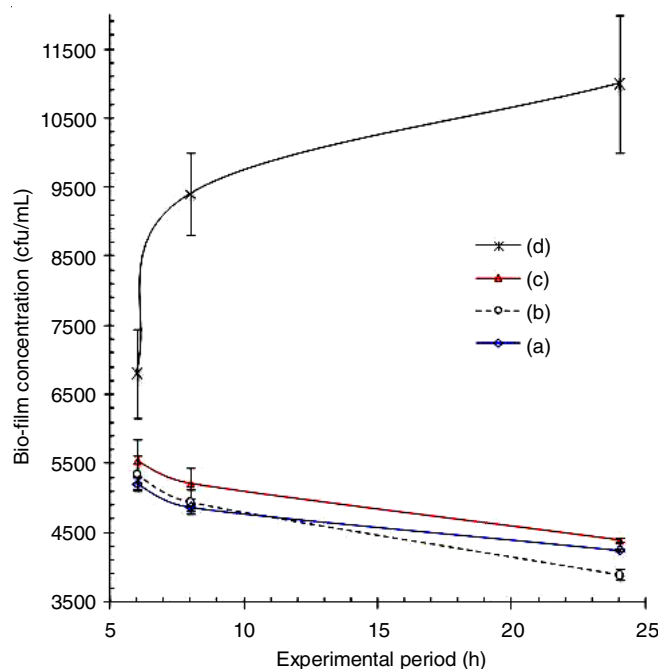


Fig. 5. Total plate count analysis result in 24 h experimental period for modified Ti-6Al-4V calcined at (a) 500 °C, (b) 600 °C, (c) 625 °C, and (d) unmodified Ti-6Al-4V

in order to suppress biofilm formation, thus preventing post-implant complication due to this biofilm.

In case of TiNTAs/Ti-6Al-4V, the surface morphology could impair bacterial adsorption. Moreover, in order to survive on such solid substrate, the bacterium needs to initiate the formation of a biofilm. For this reason, the additional changes in bacterial gene expression occurred and these results also revealed a strong influence of surface composition or the material roughness as reported earlier [22,23]. The UV activation of the modified samples plays a significant role in this case. UV activation is intended to produce a pair of charge carriers (electrons and holes) as a result of photoexcitation. These charge carriers are responsible for the formation of surface radicals, such as hydroxyl radicals and/or superoxide which are crucial for bactericidal activities. These radicals are expected to damage the cell wall of bacteria and cause its eventual death. In addition, the presence of stable oxide layer on top of Ti-based material provides a passivation region which prevents corrosion, hence increasing material stability [24].

Conclusion

Ti-6Al-4V surface modification has been successfully performed using anodization method followed by thermal treatment at various temperatures. The calcination temperature is evidently influential to both morphology and crystallite structure of TiNTAs, as well as the resultant bactericidal properties. The results showed that the anodization and thermal treatment produces nanotubular alignment of TiO₂ and converts its amorphous structure into anatase crystals. However, when the temperature is too high, destruction of the nanotubular structure is observed and the anatase structure transforms into rutile. The optimum temperature is obtained at which the crystallinity is established with the nanotubular structure remain intact. In

terms of bactericidal activities, the optimum calcination temperature of 600 °C produces a sample with the best performance of inhibiting biofilm formation. The optimum sample is capable of inhibiting biofilm five times more effective as compared to the unmodified Ti-6Al-4V.

ACKNOWLEDGEMENTS

The authors sincerely acknowledge The Directorate of Research and Community Service in Universitas Indonesia (DRPM UI) and DIKTI for the financial support (PUPT 2016 project).

CONFLICT OF INTEREST

The authors declare that there is no conflict of interests regarding the publication of this article.

REFERENCES

1. E.H. Subhaini, *Dentika Dent. J.*, **13**, 28 (2008) (In Indonesian).
2. M.A. Andrade and L.M.D.R.S. Martins, *Catalysis*, **10**, (2020); <https://doi.org/10.3390/catal10010002>
3. M. Seki, Y. Yamashita, Y. Shibata, H. Torigoe, H. Tsuda and M. Maeno, *Oral Microbiol. Immunol.*, **21**, 47 (2006); <https://doi.org/10.1111/j.1399-302X.2005.00253.x>
4. L.P. Samaranayake, *Essential Microbiology for Dentistry*, Churchill Livingstone: Hong Kong (2002).
5. G.I. Roth and R. Calmes, *Oral Biology*, CV Mosby Company: London (1981).
6. L. Le Guéhennec, A. Soueidan, P. Layrolle and Y. Amouriq, *Dent. Mater.*, **23**, 844 (2007); <https://doi.org/10.1016/j.dental.2006.06.025>
7. Y. Kirmanidou, M. Sidira, M.-E. Drosou, V. Bennani, A. Bakopoulou, A. Tsouknidas, N. Michailidis and K. Michalakis, *BioMed Res. Int.*, **2016**, 2908570 (2016); <https://doi.org/10.1155/2016/2908570>
8. G. Strnad and N. Chirila, *Proceed. Technol.*, **19**, 909 (2015); <https://doi.org/10.1016/j.protcy.2015.02.130>
9. H.J. Rack and J.I. Qazi, *Mater. Sci. Eng.*, **26**, 1269 (2006); <https://doi.org/10.1016/j.msec.2005.08.032>
10. C.N. Elias, J.H.C. Lima, R. Valiev and M.A. Meyers, *JOM*, **60**, 46 (2008); <https://doi.org/10.1007/s11837-008-0031-1>
11. A. Gallardo-Moreno, M. Pachaolivenza, L. Saldana, C. Perez-Giraldo, J. Bruque, N. Vilaboa and M. Gonzalez-Martin, *Acta Biomater.*, **5**, 181 (2009); <https://doi.org/10.1016/j.actbio.2008.07.028>
12. T. Shokuhfar, A. Hamlekhan, C. Takoudis, C. Sukotjo, M.T. Mathew, A. Virdi and S. Reza Yassar, *J. Nanotech. Smart Mater.*, **1**, 1 (2014); <https://doi.org/10.17303/jnsm.2014.1.301>
13. V. Etacheri, G. Michlits, M.K. Seery, S.J. Hinder and S.C. Pillai, *ACS Appl. Mater. Interfaces*, **5**, 1663 (2013); <https://doi.org/10.1021/am302676a>
14. A. Kedziora, W. Strek, L. Kepinski, G. Bugla-Ploskonska and W. Doroszkiwicz, *J. Sol-Gel Sci. Technol.*, **62**, 79 (2012); <https://doi.org/10.1007/s10971-012-2688-8>
15. A. Vohra, D.Y. Goswami, D.A. Deshpande and S.S. Block, *Appl. Catal. B*, **64**, 57 (2006); <https://doi.org/10.1016/j.apcatb.2005.10.025>
16. D.M. Blake, P.-C. Maness, Z. Huang, E.J. Wolfrum, J. Huang and W.A. Jacoby, *Sep. Purif. Methods*, **28**, 1 (1999); <https://doi.org/10.1080/03602549909351643>
17. H.K. Kuramitsu, X. He, R. Lux, M.H. Anderson and W. Shi, *Microbiol. Mol. Biol. Rev.*, **71**, 653 (2007); <https://doi.org/10.1128/MMBR.00024-07>
18. P.P.C. Pita, J.A. Rodrigues, C. Ota-Tsuzuki, T.F. Miato, E.G. Zenobio, G. Giro, L.C. Figueiredo, C. Gonçalves, S.A. Gehrke, A. Cassoni and J.A. Shibli, *BioMed Res. Int.*, **2015**, 159625 (2015); <https://doi.org/10.1155/2015/159625>
19. A. Jemat, M.J. Ghazali, M. Razali and Y. Otsuka, *BioMed Res. Int.*, **2015**, 791725 (2015); <https://doi.org/10.1155/2015/791725>
20. E. Matykina, A. Conde, J. de Damborenea, D.M. Marero and M.A. Arenas, *Electrochim. Acta*, **56**, 9209 (2011); <https://doi.org/10.1016/j.electacta.2011.07.131>
21. Slamet, D. Tristantini, Valentina and M. Ibadurrohman, *Int. J. Energy Res.*, **37**, 1372 (2013); <https://doi.org/10.1002/er.2939>
22. L. Hall-Stoodley, J.W. Costerton and P. Stoodley, *Nat. Rev. Microbiol.*, **2**, 95 (2004); <https://doi.org/10.1038/nrmicro821>
23. A.S.D. Al-Radha, D. Dymock, C. Younes and D. O'Sullivan, *J. Dent.*, **40**, 146 (2012); <https://doi.org/10.1016/j.jdent.2011.12.006>
24. N. Masahashi, Y. Mizukoshi, S. Semboshi, K. Ohmura and S. Hanada, *Thin Solid Films*, **520**, 4956 (2012); <https://doi.org/10.1016/j.tsf.2012.03.026>